LETTER

Non–local propagation of correlations in quantum systems with long-range interactions

Philip Richerme[1], Zhe-Xuan Gong[1], Aaron Lee[1], Crystal Senko[1], Jacob Smith[1], Michael Foss-Feig[1], Spyridon Michalakis[2], Alexey V. Gorshkov[1] & Christopher Monroe[1]

The maximum speed with which information can propagate in a quantum many-body system directly affects how quickly disparate parts of the system can become correlated[1–4] and how difficult the system will be to describe numerically[5]. For systems with only short-range interactions, Lieb and Robinson derived a constant-velocity bound that limits correlations to within a linear effective 'light cone'[6]. However, little is known about the propagation speed in systems with long-range interactions, because analytic solutions rarely exist and because the best long-range bound[7] is too loose to accurately describe the relevant dynamical timescales for any known spin model. Here we apply a variable-range Ising spin chain Hamiltonian and a variable-range XY spin chain Hamiltonian to a far-from-equilibrium quantum many-body system and observe its time evolution. For several different interaction ranges, we determine the spatial and time-dependent correlations, extract the shape of the light cone and measure the velocity with which correlations propagate through the system. This work opens the possibility for studying a wide range of many-body dynamics in quantum systems that are otherwise intractable.

Lieb–Robinson bounds[6] have strongly influenced our understanding of locally interacting, quantum many-body systems. They restrict the many-body dynamics to a well-defined causal region outside of which correlations are exponentially suppressed[8], analogous to causal light cones that arise in relativistic theories. These bounds have enabled a number of important proofs in condensed-matter physics[5,7,9–11], and also constrain the timescales on which quantum systems might thermalize[12–14] and the maximum speed that information can be sent through a quantum channel[15]. Recent experimental work has observed linear (that is, Lieb–Robinson-like) correlation growth over six sites in a one-dimensional quantum gas[16].

When interactions in a quantum system are long range, the speed with which correlations build up between distant particles is no longer guaranteed to obey the Lieb–Robinson prediction. Indeed, for sufficiently long-range interactions, the notion of locality is expected to break down completely[17]. Inapplicability of the Lieb–Robinson bound means that comparatively little can be predicted about the growth and propagation of correlations in long-range-interacting systems, although there have been several recent theoretical and numerical advances[2,3,7,17–20].

Here we report direct measurements of the shape of the causal region and the speed at which correlations propagate in an Ising spin chain and a newly implemented XY spin chain. The experiment is effectively decoherence free and serves as an initial probe of the many-body dynamics of isolated quantum systems. Within this broad experimental framework, studies of entanglement growth[21], thermalization[12,14] or other dynamical processes—with or without controlled decoherence—can be realized. Scaling such quantum simulations to larger system sizes is straightforward (Methods), unlike ground-state or equilibrium studies that typically must consider diabatic effects[22,23].

To induce the spread of correlations, we perform a global quench by suddenly switching on the spin–spin couplings across the entire chain and allowing the system to evolve coherently. The dynamics following a global quench can be highly non-intuitive; one picture is that entangled quasiparticles created at each site propagate outwards, correlating distant parts

of the system through multiple interference pathways[13]. This process differs substantially from local quenches[21], where a single site emits quasiparticles that may travel ballistically[3,13], resulting in a different causal region and propagation speed than in a global quench (even for the same spin model).

The effective spin-1/2 system is encoded into the $^2S_{1/2}|F = 0, m_F = 0\rangle$ and $|F = 1, m_F = 0\rangle$ hyperfine 'clock' states of trapped ^{171}Yb$^+$ ions, denoted $|\downarrow\rangle_z$ and $|\uparrow\rangle_z$, respectively[24]. We initialize a chain of 11 ions by optically pumping to the product state $|\downarrow\downarrow\downarrow\ldots\rangle_z$ (Fig. 1). At time $t = 0$, we quench the system by applying phonon-mediated, laser-induced forces[25–27] to yield an Ising or XY model Hamiltonian (Methods)

$$H_{\text{Ising}} = \sum_{i<j} J_{i,j} \sigma_i^x \sigma_j^x \tag{1}$$

$$H_{XY} = \frac{1}{2} \sum_{i<j} J_{i,j} \left(\sigma_i^x \sigma_j^x + \sigma_i^z \sigma_j^z \right) \tag{2}$$

where σ_i^γ ($\gamma = x, y, z$) is the Pauli matrix acting on the ith spin, $J_{i,j}$ (in cyclic frequency) is the coupling strength between spins i and j, and we use units in which Planck's constant equals 1. For both model Hamiltonians, the
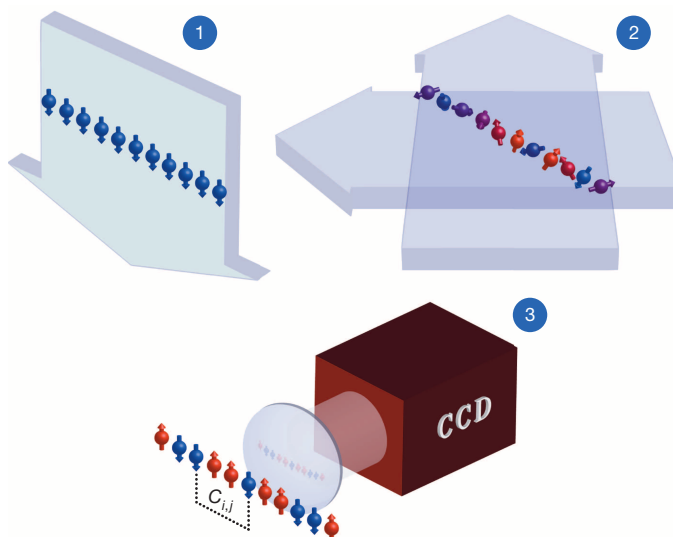
Figure 1 | Sketch of experimental protocol. Step (1): the experiment is initialized by optically pumping all 11 spins to the state $|\downarrow\rangle_z$. Step (2): after initialization, the system is quenched by applying laser-induced forces on the ions, yielding an effective Ising or XY spin chain (see text for details). Step (3): after allowing dynamical evolution of the system, the projection of each spin along the $\hat{z}$ direction is imaged onto a charge-coupled device (CCD) camera. Such measurements allow us to construct any possible correlation function $C_{i,j}$ along $\hat{z}$.

[1]Joint Quantum Institute, University of Maryland Department of Physics and National Institute of Standards and Technology, College Park, Maryland 20742, USA. [2]Institute for Quantum Information and Matter, California Institute of Technology, Pasadena, California 91125, USA.

spin–spin interaction matrix $J_{i,j}$ contains tunable, long-range couplings that fall off approximately algebraically as $J_{i,j} \propto 1/|i-j|^{\alpha}$ (ref. 26). We vary the interaction range α by adjusting a combination of trap and laser parameters[22] (Methods), choosing $\alpha \approx 0.63$, 0.83, 1.00 or 1.19 for these experiments.

After quenching to the Ising or XY model with our chosen value of α, we allow coherent evolution for various lengths of time before resolving the spin state of each ion using a charge-coupled device camera. The experiments at each time step are repeated 4,000 times to collect statistics. To observe the build-up of correlations, we use the measured spin states to construct the connected correlation function

$$C_{i,j}(t) = \left\langle \sigma_i^z(t)\sigma_j^z(t) \right\rangle - \left\langle \sigma_i^z(t) \right\rangle \left\langle \sigma_j^z(t) \right\rangle \qquad (3)$$

between any pair of ions at any time. Because the system is initially in a product state, $C_{i,j}(0) = 0$ everywhere. As the system evolves away from a product state, evaluating equation (3) at all points in space and time provides the shape of the light-cone boundary and the correlation propagation velocity for our long-range spin models.

Figure 2 shows the results of globally quenching the system to a long-range Ising model for four different interaction ranges. In each case, we extract the light-cone boundary by measuring the time it takes a correlation of fixed amplitude (here $C_{i,j} = 0.04 \approx 0.1 C_{i,j}^{\max}$, where $C_{i,j}^{\max}$ is the largest connected correlation between two ions) to travel an ion–ion separation distance r. For strongly long-range interactions ($\alpha \leq 1$), we observe accelerating information transfer through the chain. This fast propagation of correlations is not surprising, because even the direct long-range coupling between distant spins produces correlations in a time $t \propto 1/J_{i,j} \approx r^{\alpha}$. However, increasing propagation velocities quickly surpass the Lieb–Robinson velocity for a system with equivalent nearest-neighbour-only interactions, $v_{LR} = 12eJ_{\max}$, where e is Euler's number and $J_{\max}$ is the maximum Ising coupling strength for a given spin–spin coupling matrix (Fig. 2c, f, i). This serves as experimental confirmation that predictions based on the Lieb–Robinson result—including those that bound the growth of entanglement or set thermalization timescales— are no longer applicable when interactions are sufficiently long range.

For the specific case of the pure Ising model, the correlations at any time can be predicted by an exact analytic solution[18,28]:

$$\begin{aligned}
C_{i,j}(t) = &\frac{1}{2} \underset{k \neq i,j}{\Pi} \cos\left[2\left(J_{i,k}+J_{j,k}\right)t\right] \\
&+ \frac{1}{2} \underset{k \neq i,j}{\Pi} \cos\left[2\left(J_{i,k}-J_{j,k}\right)t\right] \\
&- \underset{k \neq i}{\Pi} \cos\left[2J_{i,k}t\right] \underset{k \neq j}{\Pi} \cos\left[2J_{j,k}t\right]
\end{aligned} \qquad (4)$$

In equation (4), correlations can only build up between sites i and j that are coupled either directly or through a single intermediate spin k; processes which couple through more than one intermediate site are prohibited. For instance, if the $J_{i,j}$ couplings are nearest-neighbour-only then $C_{i,j}(t) = 0$ for all $|i-j| > 2$. This property holds for any commuting Hamiltonian (Methods) and explains why the spatial correlations shown in Fig. 2 become weaker for shorter-range systems.

The products of cosines in equation (4) with many different oscillation frequencies result in the observed decay of correlations when $t \gtrsim 0.1/J_{\max}$. At later times, rephasing of these oscillations creates revivals in the spin–spin correlation. One such partial revival occurs at $t = 2.44/J_{\max}$ for $\alpha = 0.63$ (Extended Data Fig. 1), verifying that our system remains coherent on a timescale much longer than that which determines the light-cone boundary.

We repeat the quench experiments for an XY model Hamiltonian using the same set of interaction ranges α (Fig. 3). Dynamical evolution and the spread of correlations in long-range-interacting XY models are much more complex than in the Ising case because the Hamiltonian contains non-commuting terms. As a result, there exists no exact analytic solution comparable to equation (4).

Compared with the correlations observed for the Ising Hamiltonian, correlations in the XY model are much stronger at longer distances (for example, compare Fig. 2j with Fig. 3j). Processes coupling through multiple intermediate sites (which were disallowed in the commuting Ising Hamiltonian) now have a critical role in building correlations between distant spins. These processes may also explain our observation of a steeper
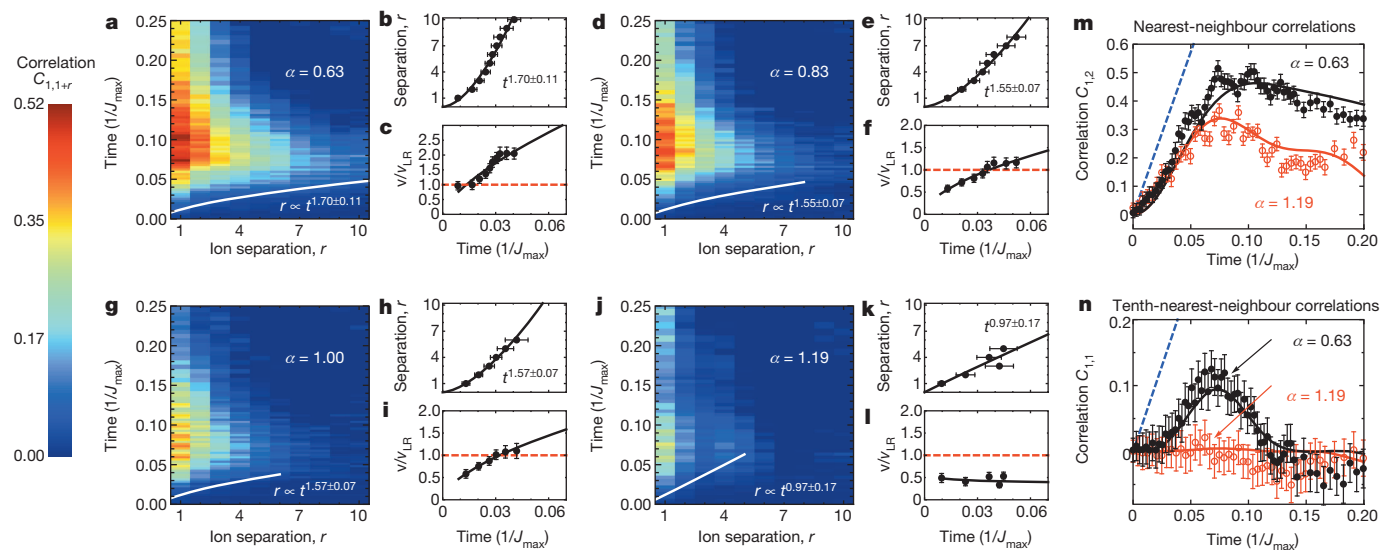
Figure 2 | Measured quench dynamics in a long-range Ising model.
a–c, Spatial and time-dependent correlations (**a**), extracted light-cone boundary (**b**) and correlation propagation velocity (**c**) following a global quench of a long-range Ising model with $\alpha = 0.63$. The curvature of the boundary shows an increasing propagation velocity (**b**), quickly exceeding the short-range Lieb–Robinson velocity bound, v_{LR} (**c**). Solid lines give a power-law fit to the data, which slightly depends on the choice of fixed contour $C_{i,j}$. **d–l**, Complementary plots for $\alpha = 0.83$ (**d–f**), $\alpha = 1.00$ (**g–i**) and $\alpha = 1.19$ (**j–l**). As the range of the interactions decreases, correlations do not

propagate as far or as quickly through the chain; the short-range velocity bound v_{LR} is not exceeded for our shortest-range interaction. **m, n**, Nearest-neighbour (**m**) and tenth-nearest-neighbour (**n**) correlations for our shortest- and longest-range interactions show excellent agreement with the decoherence-free exact solution (with no adjustable parameters) from equation (4) (solid). The dashed blue curves show an improved long-range bound valid for any commuting Hamiltonian (Methods). Error bars, 1 s.d.
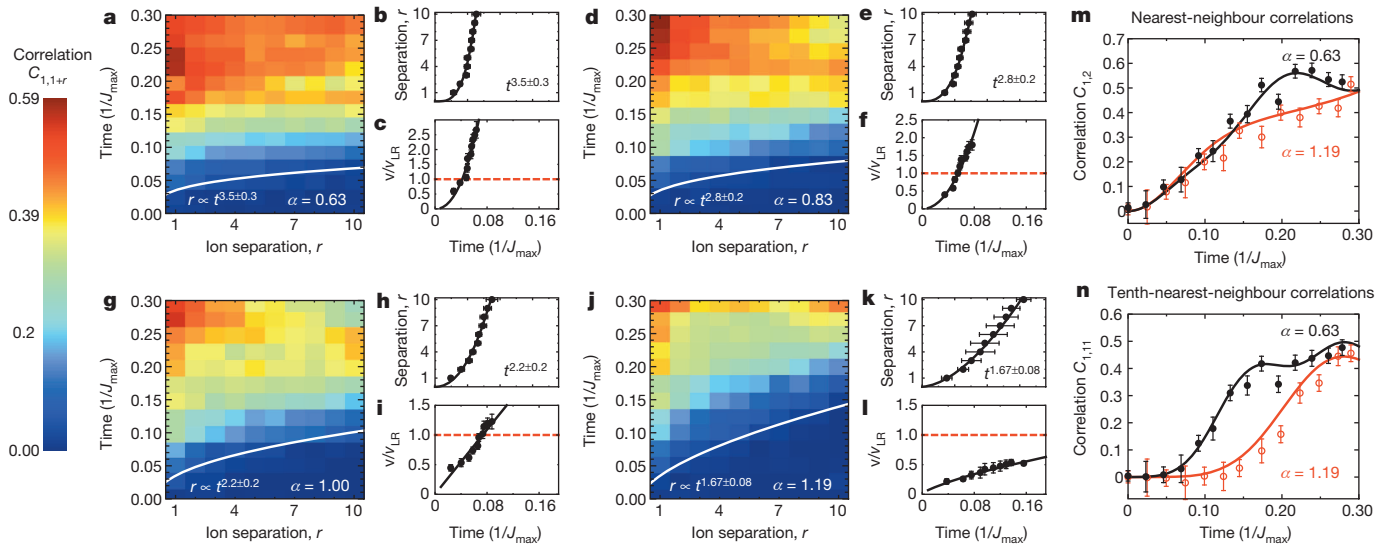
Figure 3 | Measured quench dynamics in a long-range XY model. Global quench of a long-range XY model with four different interaction ranges. **a–l**, Panel descriptions match those in Fig. 2. In each case, when compared with the Ising model, correlations between distant sites in the XY model are stronger and build up more quickly. For the shortest-range interaction (**j–l**), we observe a faster-than-linear growth of the light-cone boundary,

despite having $\alpha > 1$; no known analytic theory predicts this effect. **m**, **n**, Measured nearest-neighbour and tenth-nearest-neighbour correlations closely match the numerical solution found by evolving the Schrödinger equation of an XY model (equation (2)) with no free parameters and no decoherence. Error bars, 1 s.d.

power-law scaling of the light-cone boundary in the XY model. However, without an exact solution there is no a-priori reason to assume a power-law light-cone edge (used for the fits in Fig. 3); deviations from power-law behaviour might reveal themselves for larger system sizes.

An important observation in Fig. 3j–l is that of faster-than-linear light-cone growth for our shortest-range interaction, with $\alpha = 1.19$. Although faster-than-linear growth is expected for $\alpha < 1$ (see discussion of Ising model), there is no consensus on whether such behaviour is generically expected for $\alpha > 1$. Our experimental observation has prompted us to numerically check the light-cone shape for $\alpha = 1.19$; we find that faster-than-linear scaling persists in systems of up to 22 spins before our calculations break down (Extended Data Fig. 2).

Whether such scaling continues beyond ~30 spins is a question that, at present, quantum simulators are best positioned to answer. In Figs 2m, n and 3m, n, the excellent agreement between data and theory demonstrates that experiments produce the correct results in a regime still solvable by classical computers. For larger systems, where numerical evolution of the Schrödinger equation fails, the quality of quantum simulations could still be benchmarked against the exact Ising solution of equation (4). Finding close agreement in the Ising case would then build confidence in an XY model simulation, which cannot be validated by any other known method.

For the XY model, we additionally study the spatial decay of correlations outside the light-cone boundary. The data (Fig. 4) is well described by fits to exponentially decaying functions. Recent theoretical work[20] predicts an initial decay of spatial correlations bounded by an exponential, followed by a power-law decay; we speculate that much larger system sizes and several hundred thousand repetitions of each data point (to reduce the shot-noise uncertainty sufficiently) would be necessary to see this effect.

A perturbative treatment of time evolution under the XY Hamiltonian yields the short-time approximation for the correlation function $C_{i,j}(t) \approx (J_{i,j}t)^2$. These values are plotted as dashed lines along with the data in Fig. 4. Although the perturbative result matches the data early on, it fails to describe the dynamics at longer evolution times. The discrepancies indicate that the light-cone shapes observed in the XY model are fundamentally non-perturbative; rather, they result from the build-up of correlations through multiple intermediate sites and cannot be described by any known analytical method.
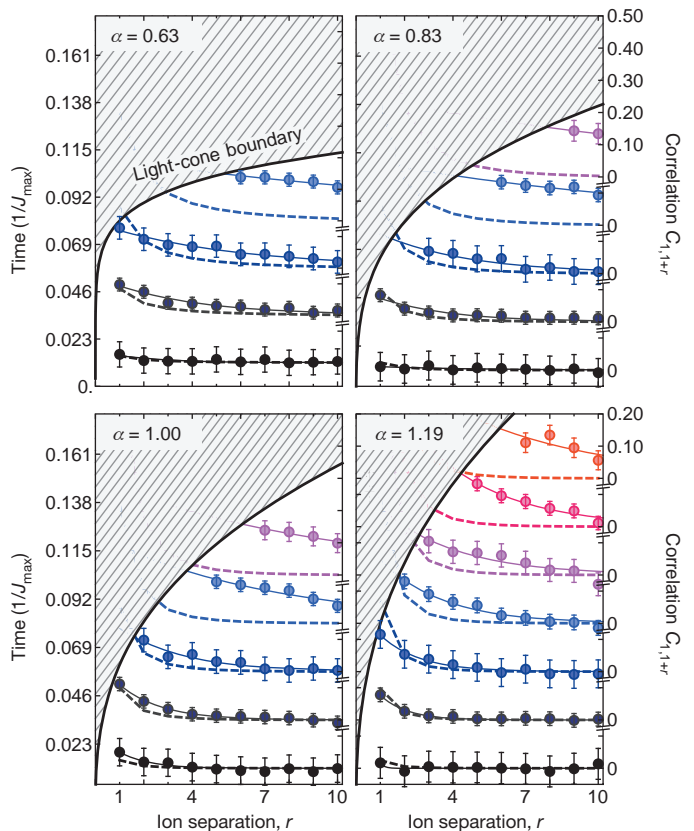
Figure 4 | Correlations and dynamics beyond the perturbative regime. Decay of spatial correlations outside the light-cone boundaries for a long-range XY model with $\alpha = 0.63, 0.83, 1.00$ or 1.19. The hatched region indicates the area inside the light-cone boundary $C_{i,j} = 0.15$. The data corresponds to times indicated by tickmarks on the left axis. Solid lines give an exponential fit to the data and dashed lines show the predictions from a perturbative calculation. Perturbation theory does not accurately describe the dynamics at later times. Associated data and theoretical results are similarly coloured to guide the eye. Error bars, 1 s.d.

We have presented experimental observations of the causal region and propagation velocities for correlations following global quenches in Ising and *XY* spin models. The long-range interactions in our system lead to a breakdown of the locality associated with Lieb–Robinson bounds, and dynamical evolution in the *XY* model leads to results that cannot be described by analytic or perturbative theory. Our work demonstrates that quantum simulators with only a few tens of spins can be an important tool for investigating and enriching our understanding of dynamics in complex many-body systems.

METHODS SUMMARY

We generate spin–spin interactions by applying spin-dependent optical dipole forces to ions confined in a three-layer linear Paul trap with a 4.8 MHz radial frequency. Two off-resonance laser beams with a wavevector difference Δk along a principal axis of transverse motion globally address the ions and drive stimulated Raman transitions. The two beams contain a pair of beat-note frequencies symmetrically detuned from the resonant transition at $v_0 = 12.642819$ GHz by a frequency μ, comparable to the transverse motional mode frequencies. In the Lamb–Dicke regime, this results in the Ising-type Hamiltonian in equation (1)[25,26] with

$$J_{i,j} = \Omega^2 \omega_R \sum_{m=1}^{N} \frac{b_{i,m} b_{j,m}}{\mu^2 - \omega_m^2}$$

where Ω is the global Rabi frequency, $\omega_R = \hbar \Delta k^2/2M$ ($\hbar$, Planck's constant divided by 2π) is the recoil frequency, $b_{i,m}$ is the normal-mode matrix[29] and ω_m are the transverse mode frequencies. The coupling profile may be approximated as a power-law decay $J_{i,j} \approx J_0/|i-j|^\alpha$, where in principle α can be tuned between 0 and 3 by varying the laser detuning μ or the trap frequencies ω_m (refs 22, 26).

We implement a tunable-range *XY* model by adding an effective transverse magnetic field $B \sum_i \sigma_i^y$ to the pure Ising Hamiltonian with an additional laser beat-note frequency at v_0. In the limit $B \gg J$, processes governed by the $\sigma_i^x \sigma_j^x$ coupling which flip two spins along y (for example $\sigma^+ \sigma^+$, where here $\sigma^\pm = \sigma^z \pm i\sigma^x$) are energetically forbidden, leaving only the energy-conserving flip-flop terms ($\sigma^+ \sigma^- + \sigma^- \sigma^+$). At times $t = n/B$ (with integer n), the dynamics of the transverse field rephases and leaves only the pure *XY* Hamiltonian of equation (2).

In the limit $B > \eta_m \Omega$, where $\eta_m = \Delta k \sqrt{\hbar/2M\omega_m}$, phonon contributions from the large, non-commuting transverse field can lead to unwanted spin–motion entanglement at the end of an experiment[30]. Therefore, this method of generating an *XY* model requires the hierarchy $J \ll B \ll \eta_m \Omega$ for all m. For our typical trap parameters, $J_{max} \approx 400$ Hz, $B \approx 4$ kHz and $\eta_m \Omega \approx 20$ kHz.

1. Nachtergaele, B., Ogata, Y. & Sims, R. Propagation of correlations in quantum lattice systems. *J. Stat. Phys.* **124,** 1 (2006).
2. Schachenmayer, J., Lanyon, B., Roos, C. & Daley, A. Entanglement growth in quench dynamics with variable range interactions. *Phys. Rev. X* **3,** 031015 (2013).
3. Hauke, P. & Tagliacozzo, L. Spread of correlations in long-range interacting quantum systems. *Phys. Rev. Lett.* **111,** 207202 (2013).
4. Hazzard, K. R. A., Manmana, S. R., Foss-Feig, M. & Rey, A. M. Far-from-equilibrium quantum magnetism with ultracold polar molecules. *Phys. Rev. Lett.* **110,** 075301 (2013).
5. Eisert, J., Cramer, M. & Plenio, M. Area laws for the entanglement entropy. *Rev. Mod. Phys.* **82,** 277 (2010).
6. Lieb, E. & Robinson, D. The finite group velocity of quantum spin systems. *Commun. Math. Phys.* **28,** 251–257 (1972).
7. Hastings, M. & Koma, T. Spectral gap and exponential decay of correlations. *Commun. Math. Phys.* **265,** 781–804 (2006).
8. Bravyi, S., Hastings, M. B. & Verstraete, F. Lieb-Robinson bounds and the generation of correlations and topological quantum order. *Phys. Rev. Lett.* **97,** 050401 (2006).
9. Nachtergaele, B. & Sims, R. Lieb-Robinson bound and the exponential clustering theorem. *Commun. Math. Phys.* **265,** 119–130 (2006).
10. Hastings, M. An area law for one-dimensional quantum systems. *J. Stat. Mech.* **2007,** P08024 (2007).
11. Michalakis, S. Stability of the area law for the entropy of entanglement. Preprint at http://arxiv.org/abs/1206.6900 (2012).
12. Rigol, M., Dunjko, V., Yurovsky, V. & Olshanii, M. Relaxation in a completely integrable many-body quantum system: an ab initio study of the dynamics of the highly excited states of 1D lattice hard-core bosons. *Phys. Rev. Lett.* **98,** 050405 (2007).
13. Calabrese, P. & Cardy, J. Time dependence of correlation functions following a quantum quench. *Phys. Rev. Lett.* **96,** 136801 (2006).
14. Gong, Z.-X. & Duan, L.-M. Prethermalization and dynamic phase transition in an isolated trapped ion spin chain. *New J. Phys.* **15,** 113051 (2013).
15. Bose, S. Quantum communication through spin chain dynamics: an introductory overview. *Contemp. Phys.* **48,** 13–30 (2007).
16. Cheneau, M. *et al.* Light-cone-like spreading of correlations in a quantum many-body system. *Nature* **481,** 484–487 (2012).
17. Eisert, J., van den Worm, M., Manmana, S. & Kastner, M. Breakdown of quasi-locality in long-range quantum lattice models. *Phys. Rev. Lett.* **111,** 260401 (2013).
18. van den Worm, M., Sawyer, B., Bollinger, J. & Kastner, M. Relaxation timescales and decay of correlations in a long-range interacting quantum simulator. *New J. Phys.* **15,** 083007 (2013).
19. Jünemann, J., Cadarso, A., Perez-Garcia, D., Bermudez, A. & Garcia-Ripoll, J. J. Lieb-Robinson bounds for spin-boson lattice models and trapped ions. *Phys. Rev. Lett.* **111,** 230404 (2013).
20. Gong, Z.-X., Foss-Feig, M., Michalakis, S. & Gorshkov, A. V. Persistence of locality in systems with power-law interactions. Preprint at http://arxiv.org/abs/1401.6174 (2014).
21. Jurcevic, P. *et al.* Quasiparticle engineering and entanglement propagation in a quantum many-body system. *Nature* http://dx.doi.org/10.1038/nature13461 (this issue).
22. Islam, R. *et al.* Emergence and frustration of magnetic order with variable-range interactions in a trapped ion quantum simulator. *Science* **340,** 583–587 (2013).
23. Richerme, P. *et al.* Quantum catalysis of magnetic phase transitions in a quantum simulator. *Phys. Rev. Lett.* **111,** 100506 (2013).
24. Olmschenk, S. *et al.* Manipulation and detection of a trapped Yb+ hyperfine qubit. *Phys. Rev. A* **76,** 052314 (2007).
25. Mølmer, K. & Sørensen, A. Multiparticle entanglement of hot trapped ions. *Phys. Rev. Lett.* **82,** 1835 (1999).
26. Porras, D. & Cirac, J. I. Effective quantum spin systems with trapped ions. *Phys. Rev. Lett.* **92,** 207901 (2004).
27. Kim, K. *et al.* Entanglement and tunable spin-spin couplings between trapped ions using multiple transverse modes. *Phys. Rev. Lett.* **103,** 120502 (2009).
28. Foss-Feig, M., Hazzard, K. R. A., Bollinger, J. J. & Rey, A. M. Nonequilibrium dynamics of arbitrary-range ising models with decoherence: an exact analytic solution. *Phys. Rev. A* **87,** 042101 (2013).
29. James, D. F. V. Quantum dynamics of cold trapped ions with application to quantum computation. *Appl. Phys. B* **66,** 181–190 (1998).
30. Wang, C.-C. J. & Freericks, J. K. Intrinsic phonon effects on analog quantum simulators with ultracold trapped ions. *Phys. Rev. A* **86,** 032329 (2012).

METHODS

Generating spin–spin couplings. We generate spin–spin interactions by applying spin-dependent optical dipole forces to ions confined in a three-layer linear Paul trap with a 4.8 MHz radial frequency. Two off-resonance laser beams with a wavevector difference Δk along a principal axis of transverse motion globally address the ions and drive stimulated Raman transitions. The two beams contain a pair of beat-note frequencies symmetrically detuned from the resonant transition at $v_0 = 12.642819$ GHz by a frequency μ, comparable to the transverse motional mode frequencies. In the Lamb–Dicke regime, this results in the Ising-type Hamiltonian in equation (1)[25,26] with

$$J_{i,j} = \Omega^2 \omega_R \sum_{m=1}^{N} \frac{b_{i,m} b_{j,m}}{\mu^2 - \omega_m^2} \qquad (5)$$

where Ω is the global Rabi frequency, $\omega_R = \hbar \Delta k^2 / 2M$ is the recoil frequency, $b_{i,m}$ is the normal-mode matrix[29] and ω_m are the transverse mode frequencies. The coupling profile may be approximated as a power-law decay $J_{i,j} \approx J_0/|i-j|^\alpha$, where in principle α can be tuned between 0 and 3 by varying the laser detuning μ or the trap frequencies ω_m (refs 22, 26).

We implement a tunable-range XY model by adding an effective transverse magnetic field $B \sum_i \sigma_i^y$ to the pure Ising Hamiltonian with an additional laser beat-note frequency at v_0. In the limit $B \gg J$, processes in the $\sigma_i^x \sigma_j^x$ coupling which flip two spins along y (for example $\sigma^+ \sigma^+$, where here $\sigma^\pm = \sigma^z \pm i\sigma^x$) are energetically forbidden, leaving only the energy-conserving flip-flop terms ($\sigma^+ \sigma^- + \sigma^- \sigma^+$). At times $t = n/B$ (with integer n), the dynamics of the transverse field rephases and leaves only the pure XY Hamiltonian of equation (2).

In the limit $B > \eta_m \Omega$, where $\eta_m = \Delta k \sqrt{\hbar/2M\omega_m}$, phonon contributions from the large, non-commuting transverse field can lead to unwanted spin–motion entanglement at the end of an experiment[30]. Therefore, this method of generating an XY model requires the hierarchy $J \ll B \ll \eta_m \Omega$ for all m. For our typical trap parameters, $J_{max} \approx 400$ Hz, $B \approx 4$ kHz and $\eta_m \Omega \approx 20$ kHz.

State detection and readout. After quenching to, and allowing time evolution under, our spin Hamiltonian, we measure the spin projections of each ion along the z direction of the Bloch sphere. For 3 ms, we expose the ions to a laser beam that addresses the cycling transition $^2S_{1/2}|F=1\rangle$ to $^2P_{1/2}|F=0\rangle$. Ions fluoresce only if they are in the state $|\uparrow\rangle_z$. This fluorescence is collected through an objective with a numerical aperture of 0.23 and imaged using an intensified CCD camera with single-site resolution.

To discriminate between 'bright' and 'dark' states ($|\uparrow\rangle_z$ and $|\downarrow\rangle_z$, respectively), we begin by calibrating the camera with 1,000 cycles each of all-bright and all-dark states. For the bright states, the projection of the two-dimensional CCD image onto a one-dimensional (1D) row gives a profile comprised of Gaussians at each ion location. We perform fits to locate the centre and fluorescence width of each ion on our CCD.

We achieve single-shot discrimination of individual ion states in the experimental data by fitting the captured 1D profile to a series of Gaussians with calibrated widths and positions but freely varying amplitudes. The extracted amplitudes for each ion are then compared with a threshold found by Monte Carlo simulation to determine whether the measured state was bright or dark. Our discrimination protocol also gives an estimate of the detection error (for example, misidentifying a bright ion as dark), which is typically of order 5%. Corrected state probabilities (along with their respective errors) are found following the method outlined in ref. 31, which also takes into account errors due to quantum projection noise.

Quantum coherence and scaling. For the data presented in Figs 2 and 3 for the Ising and XY models, correlations propagate across the entire chain in a time $t \approx 0.1/J_{max}$. During this time, we find excellent agreement between the data and decoherence-free numerical simulations. This indicates that the experiment remains coherent on the timescales needed to measure the light-cone shape and correlation propagation velocity.

To investigate coherences at longer times, we look for partial revivals of correlations as predicted by equation (4), with $\alpha = 0.63$. (Other values of α are not predicted to show partial revivals of measurable size within experimentally accessible timescales.) Extended Data Fig. 1 shows evidence that the system remains coherent until at least $t \approx 2.5/J_{max}$, substantially longer than is needed to extract the light-cone boundary for an 11-spin system.

A natural question to ask is how long it takes to observe the full light-cone boundary in an N-spin system. We may then estimate the potential for scaling to larger numbers while keeping the demonstrated coherence time and all other experimental parameters fixed. In the worst case, an Ising model with $\alpha = 1.19$, the light-cone boundary spreads across five sites in a time $t = 0.07/J_{max}$, and grows as $r \propto t^{0.97}$. If correlations were to continue spreading at this rate, they would reach nearly 100 sites away within our demonstrated $t = 2.5/J_{max}$ coherence time. If one is instead interested in seeing whether faster-than-linear growth persists at the same rate for an XY model with $\alpha = 1.19$, correlations could potentially spread over 700 sites within $t = 2.5/J_{max}$. Although technical challenges certainly must be addressed before scaling to these large sizes, we note that the state initialization, evolution, and measurement procedures implemented here would remain unchanged even for hundreds of ions.

Lieb–Robinson velocity for nearest-neighbour interactions. Here we justify our claim that the Lieb–Robinson velocity[6] for the spread of correlation functions from an initial product state, evolving under a 1D spin Hamiltonian with only nearest-neighbour interactions, is bounded above by $v_{LR} = 12eJ$. In particular, we consider a Hamiltonian

$$H = \sum_j h_{j,j+1}$$

with interaction strength $||h_{j,j+1}|| = J$. Note that both the Ising and XY Hamiltonians defined in the manuscript satisfy these assumptions in the $\alpha \to \infty$ limit, where $J_{ij} = J\delta_{j,i+1}$, as can easily be checked by calculating $\left\| \sigma_i^x \sigma_j^x \right\| = \left\| \sigma_i^x \sigma_j^x + \sigma_i^z \sigma_j^z \right\| / 2 = 1$. For operators evolving in the Heisenberg picture under H (such that $A(t) \equiv e^{iHt}A(0)e^{-iHt}$), we would like to compute the connected correlation function

$$C_{i,j}(t) = \left\langle A_i(t) B_j(t) \right\rangle_c$$
$$\equiv \left\langle A_i(t) B_j(t) \right\rangle - \left\langle A_i(t) \right\rangle \left\langle B_j(t) \right\rangle$$

where A_i and B_j are supported on sites i and j, respectively.

A bound on these correlation functions follows immediately from results in ref. 8, which relate a Lieb–Robinson bound on unequal-time commutators to a bound on connected correlation functions. In particular, for a Lieb–Robinson commutator bound of the form

$$\left\| \left[A_i(t), B_j(0) \right] \right\| \le c \|A_i\| \|B_j\| e^{(vt-r)/\xi}$$

we have

$$C_{i,j}(t) \le 4c \|A_i\| \|B_j\| e^{(vt-r/2)/\xi} \qquad (6)$$

where r is the distance between the two sites i and j.

The Lieb–Robinson commutator bound for a nearest-neighbour Hamiltonian on a D-dimensional square lattice is given by[8]

$$\left\| \left[A_i(t), B_j(0) \right] \right\| \le 2 \|A_i\| \|B_j\| \sum_{k=r}^{\infty} \frac{(2Jt(4D-1))^k}{k!}$$

which in 1D gives

$$\left\| \left[A_i(t), B_j(0) \right] \right\| \le 2 \|A_i\| \|B_j\| e^{-r} \sum_{k=r}^{\infty} \frac{(6eJt)^k}{k!}$$
$$\le 2 \|A_i\| \|B_j\| e^{6eJt-r}$$

and, hence, $v = 6eJ$. The velocity bound for the spreading of correlations is obtained by setting the bound on $C_{ij}(t)$ (the right-hand side of equation (6)) to a constant value and solving $r = v_{LR}t$, which yields $v_{LR} = 2v = 12eJ$.

Bound for commuting Hamiltonians. Motivated by applications to the Ising model studied in the manuscript, here we derive a bound applicable to 1D Hamiltonians

$$H = \sum_{k<l} h_{kl}$$

where $[h_{kl}, h_{k'l'}] = 0$ for any k, l, k', l'. As above, we are interested in bounding the connected correlation function $C_{i,j}(t)$, and without loss of generality we take $i < j$. For convenience in what follows, we define $h_{kk} = 0$, and take $h_{kj} = h_{jk}$ (even though only one of the two appears in the Hamiltonian).

To compute $A_i(t)$, let us first define $H_i = \sum_k h_{ik}$ as the part of H that (in general) does not commute with A_i, so that $A_i(t) = e^{iH_i t} A_i e^{-iH_i t}$. We can further separate H_i into two parts by choosing a site index k_0 satisfying $i \le k_0 < j$ and writing

$$H_i' = \sum_{k \le k_0} h_{ik}$$
$$H_i'' = \sum_{k > k_0} h_{ik}$$

As a result

$$A_i(t) = e^{iH_i' t} e^{iH_i'' t} A_i e^{-iH_i'' t} e^{-iH_i' t}$$
$$= e^{iH_i' t} \left(A_i + \int_0^t d\tau \left[e^{iH_i'' \tau} A_i e^{-iH_i'' \tau}, H_i'' \right] \right) e^{-iH_i' t}$$
$$\equiv A_i'(t) + f_i(t)$$

where $A_i'(t) = e^{iH_i' t} A_i e^{-iH_i' t}$ and

$$\|f_i(t)\| \le 2t \|A_i\| \|H_i''\|$$

Similarly, we can define

$$H'_j = \sum_{k > k_0} h_{jk}$$

$$H''_j = \sum_{k \leq k_0} h_{jk}$$

and $A'_j(t) = e^{iH'_j t} A_j e^{-iH'_j t}$, such that $A_j(t) = A'_j(t) + f_j(t)$ and

$$\left\| f_j(t) \right\| \leq 2t \left\| A_j \right\| \left\| H''_j \right\|$$

In terms of these newly defined quantities, we can write

$$C_{i,j}(t) = \left\langle A'_i(t) A'_j(t) \right\rangle_c + \left\langle f_i(t) A_j(t) \right\rangle_c + \left\langle A'_i(t) f_j(t) \right\rangle_c$$

where we note that the second term contains $A_j(t)$ (rather than $A'_j(t)$). By inspection, $\left\langle A'_i(t) A'_j(t) \right\rangle_c = 0$. Using the bounds on $\|f_i(t)\|$ and $\|f_j(t)\|$, together with the inequality $|\langle AB \rangle_c| \leq 2\|A\|\|B\|$, we find that

$$\left| C_{i,j}(t) \right| \leq 4t \|A_i\| \|A_j\| \left(\|H''_i\| + \|H''_j\| \right)$$

Noting that $|J_{kl}| = \|h_{kl}\|$, we then have

$$\left| C_{i,j}(t) \right| \leq 4t \|A_i\| \|A_j\| \left(\sum_{k > k_0} |J_{ik}| + \sum_{k \leq k_0} |J_{jk}| \right)$$

One can optimize the value of k_0 to give the tightest bound. For power-law couplings $J_{kl} \approx |k - l|^{-\alpha}$ ($\alpha > 0$) in 1D, choosing k_0 right in the middle of i and j will generally give the tightest bound.

Multi-hop processes are forbidden for commuting Hamiltonians. Here we prove the claim that, given an initial product state evolving under a commuting Hamiltonian, distant spins can only become correlated if they are either directly coupled or if they share an intermediate spin to which they both couple; multi-hop processes (for example site A coupling to site D through sites B and C) do not occur.

We consider the time evolution of the operators A_i and A_j, residing on sites i and j of the lattice. As discussed in the previous section, the time evolution of A_i and A_j can be written as

$$A_i(t) = e^{iH_i t} A_i e^{-iH_i t}$$

$$A_j(t) = e^{iH_j t} A_j e^{-iH_j t}$$

where

$$H_i = \sum_p h_{ip}$$

$$H_j = \sum_q h_{jq}$$

We can expand the time-evolution operator to obtain

$$\begin{aligned} A_i(t) &= A_i + ih[H_i, A_i] - \frac{t^2}{2!}[H_i, [H_i, A_i]] + \dots \\ &= A_i + it \sum_{p1} [h_{ip1}, A_i] - \frac{t^2}{2!} \sum_{p1, p2} [h_{ip2}, [h_{ip1}, A_i]] + \dots \end{aligned} \tag{7}$$

It follows from equation (7) that $A_i(t)$ is supported on (that is, can be written in terms of operators belonging to) site i and any site p for which $\|h_{ip}\| \neq 0$; we denote the set of such points by Λ_i, and define an equivalent set Λ_j containing all sites supporting the operator $A_j(t)$. If $\|h_{ij}\| = 0$ and there are no sites p that simultaneously satisfy $\|h_{ip}\| \neq 0$ and $\|h_{jp}\| \neq 0$, then $\Lambda_i \cap \Lambda_j = \emptyset$. In this case, it is clear that an initial product state must satisfy $\langle A_i(t) A_j(t) \rangle = \langle A_i(t) \rangle \langle A_j(t) \rangle$, and therefore any connected correlation function $C_{i,j}(t)$ must vanish.

Numerical solutions. Because no analytic solution exists for the XY model, exact long-time dynamics (where the perturbative results derived above break down) must be obtained by numerical solution of the Schrödinger equation. The curves presented in Fig. 3m, n are calculated using a standard numerical integration routine. With our experimental spin–spin couplings J_{ij} as inputs (equation (5)), we construct the full XY Hamiltonian (equation (2)) using sparse matrices. After evolving the initial product state $|\psi(0)\rangle$ under the Hamiltonian H_{XY} for a time t, we construct the desired correlation functions by calculating

$$C_{i,j}(t) = \left\langle \psi(t) \left| \sigma_i^z \sigma_j^z \right| \psi(t) \right\rangle$$
$$- \left\langle \psi(t) \left| \sigma_i^z \right| \psi(t) \right\rangle \left\langle \psi(t) \left| \sigma_j^z \right| \psi(t) \right\rangle$$

To numerically check the light-cone shape when $\alpha = 1.19$ in a system of 22 spins, we follow a similar procedure to calculate the time-evolved state $|\psi(t)\rangle$. The results of this calculation are shown in Extended Data Fig. 2. Note that faster-than-linear growth of the light-cone boundary persists in this larger system of 22 spins.

Short-time perturbation theory for the XY model. Unlike in the Ising model, no exact analytic solution exists for the XY model (even in 1D, owing to the long-range couplings). However, we can nevertheless expand the time-evolution operator to low order and thereby recover the dynamics at short times. At sufficiently long times, this perturbative expansion (carried out here to second order) becomes a poor approximation. This failure, which is observed in the experimental dynamics (Fig. 4), suggests that the growth of correlations at long distances is not the result of direct spin–spin interactions; instead those correlations originate from the repeated propagation of information through intermediate spins.

We are interested in the time evolution of a connected correlation function $C_{i,j}(t) = \langle A_i(t) A_j(t) \rangle_c$ of observables A_i and A_j located at different sites i and j. To second order in time, we have

$$A_i(t) = A_i + it[H, A_i] - \frac{t^2}{2!}[H, [H, A_i]] + \mathcal{O}(t^3)$$

which yields

$$\begin{aligned} & \left\langle A_i(t) A_j(t) \right\rangle_c \\ &= \langle A_i A_j \rangle_c + it \left(\left\langle A_i [H, A_j] \right\rangle_c + \left\langle [H, A_i] A_j \right\rangle_c \right) \\ &\quad - \frac{t^2}{2} \left(\left\langle A_i [H, [H, A_j]] \right\rangle_c + \left\langle [H, [H, A_i]] A_j \right\rangle_c \right) \\ &\quad - t^2 \left\langle [H, A_i][H, A_j] \right\rangle_c + \mathcal{O}(t^3) \end{aligned} \tag{8}$$

Note that in equation (8) we use the notation

$$\langle A_i[H, A_j] \rangle_c = \langle A_i[H, A_j] \rangle - \langle A_i \rangle \langle [H, A_j] \rangle$$

In the experiment, where A_i corresponds to the Pauli spin operator σ_i^z, the initial state is (1) a product state $|\downarrow \cdots \downarrow\rangle_z$ and (2) a simultaneous eigenstate of each A_i. As a result of (1), the connected correlation at $t = 0$ vanishes ($\langle A_i A_j \rangle_c = 0$). As a result of (2), the third and fourth lines in equation (8) vanish. Therefore, we have

$$\left\langle \sigma_i^z(t) \sigma_j^z(t) \right\rangle_c = -t^2 \left\langle [H, \sigma_i^z][H, \sigma_j^z] \right\rangle_c + \mathcal{O}(t^3)$$

For the XY Hamiltonians we find

$$[H, \sigma_i^z] = -i \sum_{k \neq i} J_{ik} \sigma_i^y \sigma_k^x$$

and so

$$\begin{aligned} & \left\langle \sigma_i^z(t) \sigma_j^z(t) \right\rangle_c \\ &= t^2 \sum_{k \neq i, l \neq j} J_{ik} J_{jl} \left(\left\langle \sigma_i^y \sigma_k^x \sigma_j^y \sigma_l^x \right\rangle - \left\langle \sigma_i^y \sigma_k^x \right\rangle \left\langle \sigma_j^y \sigma_l^x \right\rangle \right) \\ &\quad + \mathcal{O}(t^3) \end{aligned} \tag{9}$$

Because the initial state is polarized along z, the only term that has a non-zero expectation value on the right-hand side of equation (9) is the one with $k = j$ and $l = i$. Therefore
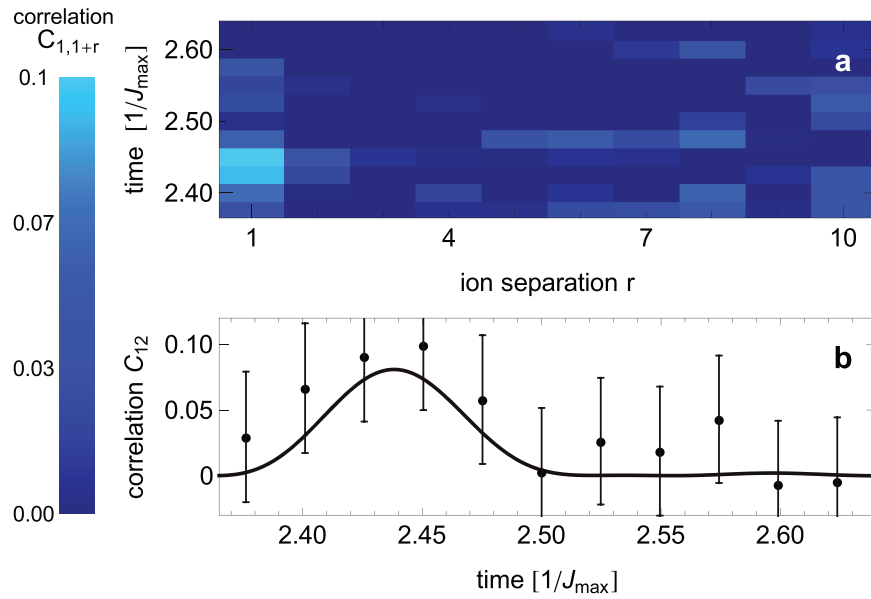
$$\begin{aligned} \left\langle \sigma_i^z(t) \sigma_j^z(t) \right\rangle_c &= t^2 J_{ij}^2 \left\langle \sigma_i^y \sigma_j^x \sigma_j^y \sigma_i^x \right\rangle + \mathcal{O}(t^3) \\ &= t^2 J_{ij}^2 \left\langle \sigma_i^z \sigma_j^z \right\rangle + \mathcal{O}(t^3) \\ &= (J_{ij} t)^2 + \mathcal{O}(t^3) \end{aligned}$$

which is the short-time result used in the main text.

31. Shen, C. & Duan, L.-M. Correcting detection errors in quantum state engineering through data processing. *New J. Phys.* **14**, 053053 (2012).

Extended Data Figure 1 | A long-time partial revival in the long-range Ising model. a, Spatial correlations measured at long times after a global quench of an Ising model with $\alpha = 0.63$. **b**, A small partial revival in correlation between sites 1 and 2 is evident, showing quantum coherence at long times. The black line shows the exact solution predicted from equation (4). Error bars, 1 s.d.
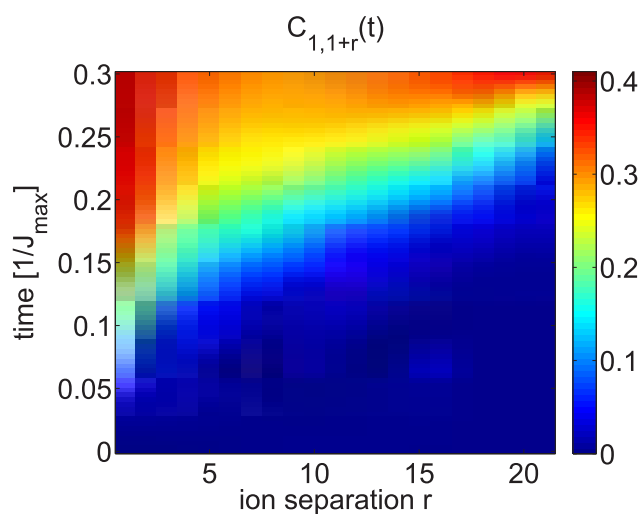
Extended Data Figure 2 | Numeric calculation of *XY* model correlations.
Calculated spatial and time-dependent correlations for an $N = 22$-spin *XY*
model with spin–spin couplings $J_{ij} \approx J_0/|i-j|^{1.19}$, found by numerically
evolving the Schrödinger equation.